1.

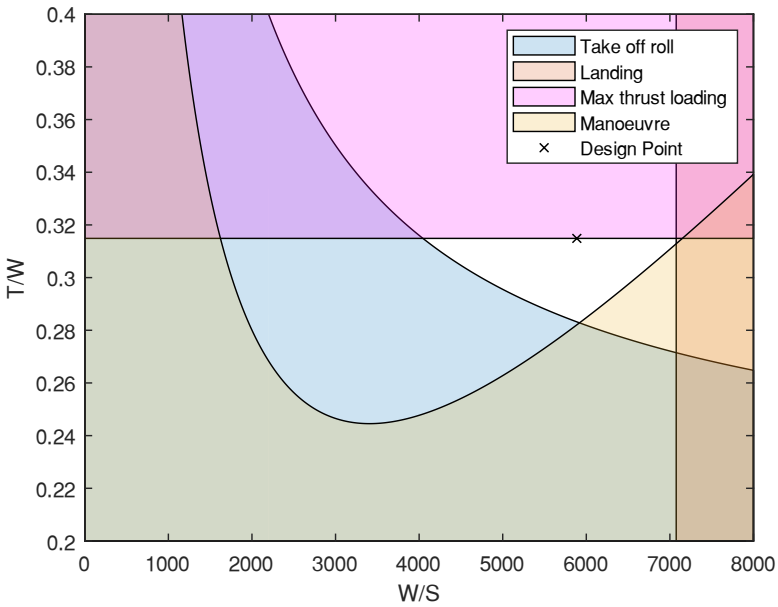

Figure 2.1.1: Constraint diagram of the aircraft

2. a.

Table 2.2.1: Parameters used in the analysis of the aircraft.

Speed (ms^{-1})	**Root Reynolds Number**	**Tip Reynolds Number**	**Density (kgm^{-3})**	**Temperature (°C)**	**Viscosity (m^2s^{-1})**	
230.412	71,595,106	21,452,685	0.562	-56.0	Kinematic	Dynamic
					1.783e-05	1.00e-05

The speed was calculated using the speed of sound at the cruise altitude of 35,000 feet which is 295.4 ms^{-1} [5] which is then multiplied by the cruise Mach number 0.79 which gives the speed 230.412 ms^{-1}. The root and tip Reynolds numbers, density and viscosity were calculated in XFLR5. The temperature at 35,000 feet was obtained from an online source [5].

b.

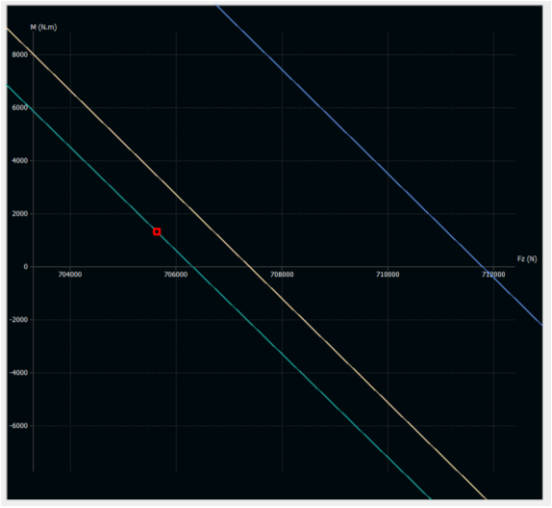

Figure 2.2.1: Moment (Nm) vs. F_Z (N) graph of trimmed aircraft (green) with elevator angle -0.2047 at angle of attack (red dot) compared to elevator -2.05 (blue) and elevator -2.05 (beige)

c. The main wing tilt angle is set at 0 degrees and the elevator tilt angle is set at -2.0247 degrees. The overall aircraft angle of attack is 3.08 degrees because the lift coefficient at this value of α is 0.396 which is approximately equal to the calculated value of the lift coefficient during steady and level flight.

d. Table 2.2.2: Summary of number of panels and distribution type used for the right side of the wing.

	X - panel no.	X - distribution	Y - panel no.	Y - distribution
NACA 1812 (main wing)	31	Cosine	35	Uniform
NACA 0010 (elevator)	11	Cosine	13	Uniform

The total number of VLM panels used was 809. The number of VLM panels in the main wing was 494 and in the elevator was 266. Table 2.2.2 above states the number of panels and distribution used in the chordwise (X) and streamwise (Y) directions for the respective aerofoils used in the main wing and elevator. The number of panels were first increased from the default values to produce a more accurate analysis. Then the number of panels in the X and Y directions were not varied greatly to avoid the problem of instability in the analysis. The arrangement of the panels was also taken into consideration where calculation was done to align the panels and control points of the main wing and elevator. This is to avoid having the control point on the tail surface close to the trailing leg of one of the wings horseshoe vortices. This would lead to a division by zero resulting in inconsistent results [6]. The semispan of the main wing, 16.665m was divided by the number of panels, 35, to obtain the panel length of approximately 0.476m. This panel length was divided by the semispan of the elevator 6.2 to obtain the number of panels in the elevator which is 13 as seen in Table 2.2.2 above. Therefore, the possible problem stated above is avoided and the panel density is justified.

A cosine distribution was used in the X direction. This is because it provides a higher density of panels around the leading and trailing edges of the wing. A uniform distribution in the X direction is not recommended because it does not give a high density of panels around the stated edges of the wing which is not desired as it would not be suitable. A uniform distribution was used in the Y direction. A sine or negative sine distribution was not used because there is a possible problem that could arise with these distributions. Non-physical results and instability of the results could occur if size of the panels is below the lower limit [6] which is likely to occur with a sine distribution. Therefore to mitigate against this issue, a uniform distribution was used. There is still a high density of panels along the leading and trailing edges with the uniform distribution and it is possible to carry out the panel length calculations stated above with a uniform distribution unlike with a sine distribution.

The analysis used was Fixed speed and Ring Vortex method (VLM2). The speed it was analysed at was the cruise speed of 230.412ms^{-1}. Since the aircraft is being trimmed for longitudinal static stability, the analysis chosen was fixed speed. The temperature and density were set for the specified cruise altitude and shown in Table 2.2.1.

3. The overall angle of attack of the aircraft in trimmed condition during cruise is 3.08 degrees as mentioned in Q2c. The aircraft was trimmed by changing the elevator angle to -2.0247 degrees and keeping the main wing tilt angle at 0 degrees. The lift coefficient for steady and level trimmed flight is approximately 0.395 which is what the induced and viscous drag coefficients were calculated for. It was calculated for the trimmed condition of the aircraft in Q2 where there is zero moment produced when it produces lift equal to the MTOW.

To calculate the viscous drag coefficient, a ring vortex (VLM2) analysis with polar type 1 of fixed speed was carried out in XFLR5 for a range of angles of attack from -5 to 5 with an increment of 0.1. A graph was plotted of $C_{d_{viscous}}$ against the lift coefficient C_l. The viscous drag coefficient value taken was at the lift coefficient value of the aircraft in cruise at the trimmed condition. The C_l value is 0.395 and the corresponding $C_{d_{viscous}}$ value is 0.0073 as stated in Table 2.3.5. When calculating viscous drag, the viscous regions of the wing include the boundary layer and the wake layer. However, XFLR5 considers the near-field viscous drag to be equal to the viscous drag because it only includes it in the boundary layer and not the wake layer. Therefore, the wake component will be considered in the pressure drag. Viscous drag arises from the stresses on the surface of the wing and in the boundary layer [7] . If a body is streamlined as seen in this case where it is an aerofoil, it will be dominated by viscous drag forces compared to the other drag components. This is because the viscous forces in the boundary layer are greater than the induced

lift drag forces and pressure drag forces. In Table 2.3.5 it shows that the coefficient of viscous drag is the largest value among the drag components and is therefore justified since the body is streamlined it will have a greater viscous drag force.

Induced drag is drag that arises from the development of lift. As the aircraft passes through air, the wing experiences low pressure at the top of the wing and a higher pressure at the bottom of the wing. Due to the imbalance in pressure, it will seek equilibrium causing the higher pressure to meet with the lower pressure of flowing air at the trailing edge of the wing. This produces wing vortices at the wing tips leading to downwash. The increased downwash causes the lift vector to tilt backwards which causes the induced drag. Therefore, induced drag is proportional to lift which means that during flight conditions like take-off where great amounts of lift is being generated, there will be greater amounts of induced drag. At higher angles of attack there is also greater pressure difference between the top and bottom surfaces of the wing which creates more tip vortices and will subsequently increase the downwash which increases the rearward component of lift increasing the induced drag component [8]. However in cruise, the angle of attack is kept low and there is not as much lift being generated as in take-off therefore the value of induced drag obtained which is 0.0054 as stated in Table 2.3.5 is justified as it is not the largest value but also not the smallest. The induced drag coefficient C_{d_i} was found to have a value of 0.0054 at a lift coefficient C_l value of 0.395 which is at steady and level flight. This was done by using the same method as finding the viscous drag coefficient.

Pressure drag is the drag that arises from the eddying motions that are set up in the fluid by the passage of the body [9]. In this case, the body is a streamlined aerofoil. The main wing tilt is set at an angle of 0 degrees which means that the angle of attack of the aircraft is the angle that will determine whether the flow is attached or detached. For the flow to be attached, there should be no separation between the flow and the body. This is because at small angles of attack the flow remains attached for throughout the whole chord length as the boundary layers only experience a mild pressure gradient. However, at higher angles of attack the pressure gradient increases and it produces separated flow. This is not to be considered because during cruise the aircraft is in steady and level trimmed flight which means that the angle of attack will remain low and therefore there is no separation in the flow. This can be represented by a plot of the pressure coefficient C_p against the chord length in Figure 2.3.1. It can be seen that there is no sharp decrease in the pressure coefficient and it gradually decreases to zero as it reaches the end of the chord. This shows that there is no separation in the flow. Therefore, it can be assumed that the pressure drag is equal to zero in this circumstance.

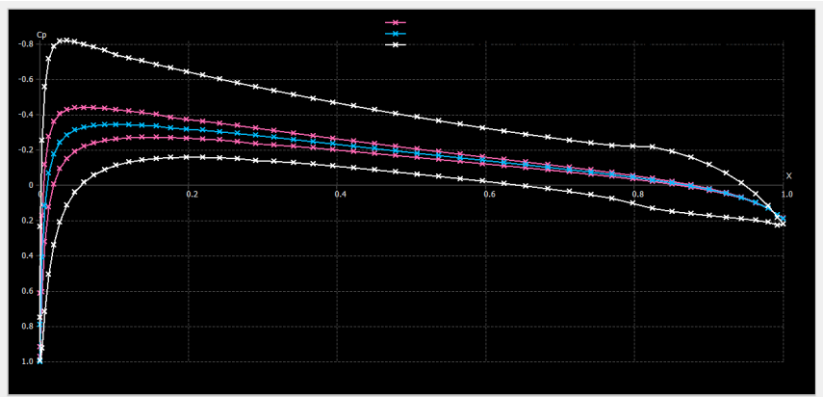

Figure 2.3.1: Pressure Coefficient graph showing no separation of flow for main wing(white), elevator(pink), and fin(blue).

Table 2.3.2: Summary of values calculated to obtain $M_{crit_{2D}}$.

		Reynolds no.	C_l	**Local** α	$C_{p_{min}}$	$M_{crit_{2D}}$
NACA 1812	Main Wing	46,523,896	0.403	3.08	-0.81828	0.639198
NACA 0010	Elevator	27,785,105	0.075	1.055	-0.43972	0.7339074
	Fin	46,523,896	0	0	-0.34303	0.76697995

Table 2.3.3: Sweep angles and areas.

	Sweep angle (°)	Area (m^2)
Main wing	27.674873	119.99
Elevator	32.828541	26.66
Fin	39.805571	24.00

$$\frac{C_{p_{min}}}{\sqrt{1-M_{crit}^2}} = \frac{2}{\gamma M_{crit}^2}\frac{\left(1+\frac{\gamma-1}{2}M_{crit}^2\right)^{\frac{\gamma}{\gamma-1}}}{1.895} - 1 \quad (1)$$

$$M_{crit_{3D}} = \frac{M_{crit_{2D}}}{\cos(\theta)} \quad (2)$$

$$C_{D_w} = K_w(M - M_{crit})^4 \quad (3)$$

The $M_{crit_{2D}}$ is adjusted for the leading-edge sweep of each of the main wing, elevator, and fin. This is done using Equation 2 [10] below where the sweep angle is taken into consideration to find the $M_{crit_{3D}}$ where θ= sweep angle the values are given in Table 2.3.3.

Table 2.3.4: Values of $M_{crit_{2D}}$ and $M_{crit_{3D}}$ to obtain wave drag coefficient.

	$M_{crit_{2D}}$	$M_{crit_{3D}}$	C_{D_w}
Main Wing	0.63919800	0.7217704	0.000149457798
Elevator	0.73390740	0.8733908	-
Fin	0.76697995	0.9983841	-

The wave drag coefficient C_{d_w}could not be calculated using XFLR5 therefore a set of numerical calculations were carried out in order to estimate the value of the wave drag coefficients for the main wing, elevator, and fin. To obtain the value of C_l that each component experiences at cruise, they were isolated, and separate analyses were run for each component: main wing, elevator and fin and the value of C_l taken was at the local angle of attack that each component experiences. The fin was analysed at C_l = 0 because the fin does not produce any lift during cruise. The main wing had a C_l value of 0.403 and elevator 0.075. Since the elevator was isolated completely it is justified that it has such a low lift coefficient. The values are reported in Table 2.3.2. Using these values of C_l an XFOIL direct analysis of each aerofoil was run at the Reynolds number at mid span to obtain the minimum pressure coefficient of each aerofoil (NACA 1812 and NACA 0010) at the specified lift coefficient value obtained previously. This direct analysis was also run at Mach number of 0 because XFOIL can only run analyses in the subsonic region however the aircraft is cruising in the transonic region. Therefore, to obtain more accurate results the analyses were run using Mach 0. The values obtained are also reported in Table 2.3.2.

After obtaining the $C_{p_{min}}$ values, Equation 1 [11] was used to obtain the M_{crit} value corresponding to each $C_{p_{min}}$ value. The elevator and fin share the same aerofoil however they have different values of C_l therefore different values of $C_{p_{min}}$ and M_{crit}. However, an assumption made is that XFLR5 only analyses the aerofoil which means that it does not take into consideration the leading-edge sweep angle of each component. Therefore, the value of M_{crit} must be adjusted for leading edge sweep angle which is done using Equation 2 to obtain the $M_{crit_{3D}}$ value. This is then used in Equation 3 [12] to obtain the wave drag coefficient, C_{D_w} , value for each component. In the equation the constant K_w is approximated to be 13 because it is slightly more than the median possible values of K_w to which it can account for any other small amounts of drag that may have been looked over. It is seen in Table 2.3.4 that the $M_{crit_{3D}}$ values for the elevator and fin are greater than the cruise Mach number of 0.78. This means that there will be no wave drag since the Mach number that the component is experiencing is greater than the cruise Mach number.

After obtaining the drag coefficients, they are dimensionalised using Equation 4 below. Where $\rho = 0.562\ kgm^{-2}$ is the density of the air at cruise altitude, $V = 240.314\ ms^{-2}$ is the velocity of the aircraft during cruise and $S =$

$119.99\ m^2$ is the main wing reference area. The values of the drag coefficients and their respective dimensionalised drag values are reported in Table 2.3.5 below.

$$D = \frac{1}{2}\rho V^2 S C_D \tag{4}$$

Table 2.3.5: Summary of drag coefficients and drag for value for each drag component and the total drag.

	Drag coefficients	**Drag (N)**
Induced	0.0054	9666.2
Viscous	0.0073	13067.3
Wave	0.000149	267.535
Pressure	0.00	0.0
Total drag		**23000.98**

The total drag is calculated to be 23000.98 N as seen in Table 2.3.5. The thrust provided by the 2 aircraft engines total to 222411.08 N. This means that the total drag experienced by the aircraft during cruise is approximately 10.34% of the total available thrust. For an aircraft that has similar maximum take-off weight and thrust as well as wing design characteristics like the Airbus A320, its thrust during cruise at an altitude of 35,000ft and Mach number 0.8 is approximately 5000 lbs [13] which is 22,241 N which is similar to the amount of drag experienced by this trimmed aircraft in cruise at the same altitude and similar Mach number. This justifies the value of total drag obtained for this trimmed aircraft.

However, there were many assumptions made during the calculation of this value of drag which could account for errors in the value. These include adjustments to the Mach number used to obtain the value of the minimum pressure coefficient in the XFOIL analysis as the Mach number 0.78 at cruise is closer to the transonic range to which if run in XFOIL will not produce as accurate results as it is better in subsonic regions. The critical Mach number is also adjusted for leading edge sweep of the main wing, elevator and fin to which inaccuracies can arise from. These are minor issues that do not heavily contribute to the reliability of the total drag value. Therefore, the overall analysis of the total drag value is reliable as it has been justified by comparing it with a similar aircraft. With the drag being roughly 10% of the total available thrust in cruise, the aircraft is able to perform efficiently during the flight. It could afford to fly at a higher cruise speed if it is experiencing low amounts of drag at this speed.

4. To calculate the static margin of the aircraft Equation 5 was used. The values obtained are reported in Table 2.4.1 below. As the percentage is almost 50% the elevator authority of the aircraft is very poor

$$Static\ margin = neutral\ point - centre\ of\ gravity \tag{5}$$

Table 2.4.1: Summary of values required.

Neutral point (m)	18.9
Centre of gravity (m)	16.977
Static margin (m)	1.923
MAC	3.948
% of MAC	48.7%

Table 2.4.2: Reporting the natural frequencies, damping ratio, time constant and eigenvalue of the aircraft modes for the trimmed aircraft.

	Aircraft Modes	**Natural frequency (Hz)**	**Damping ratio**
Longitudinal	Short period	0.743471	0.347696
	Phugoid	0.00920179	0.0213786
Lateral	Dutch Roll	0.643293	0.147088
		Time Constant	**Eigenvalue**
	Roll Subsidence	0.242885	-4.1172 + 0.00i
	Spiral	446.637	-0.0022 + 0.00i

The stability modes were obtained for the trimmed aircraft in cruise. The values obtained are reported in Table 2.4.2. Overall, the aircraft modes are dynamically stable because as seen in Table 2.4.2 the damping ratios are all positive which is an indication of dynamic stability. This is also justified by the poles being in the top left corner of the s-plane with the point on the negative plane is just a reflection of that of the positive imaginary value.

The handling characteristics of the aircraft modes are discussed to assess the stability of the trimmed baseline aircraft. These are concerned with the short term and long-term handling characteristics. The short-term characteristics are defined as the short period dynamics modes and their influence on manoeuvrability. The long-term handling characteristics are defined as the ability to maintain the trimmed equilibrium state which is influenced by the long period dynamic modes [14]. The longitudinal short-term characteristics include the short period mode and the phugoid mode. The acceptable limits for the damping ratio of the short period mode are to be between 0.3 and 2 [14]. Therefore, the damping ratio of the short period mode is acceptable. It also states that the phugoid dynamics are acceptable if the mode is stable and the damping ratio is greater than 0.04. The lateral directional dynamic stability is comprised of the roll subsidence mode, spiral mode, and Dutch roll mode. The roll subsidence mode is crucial in determining the handling characteristics. The time constant of this aircraft's roll subsidence mode is 0.2s which is less than the maximum time constant of 1.4s [14] therefore it is handleable. The spiral mode's degree of instability is related to its time to double bank angle which for this aircraft is 309s which is much larger than the minimum value stated by Cook for an aircraft in cruise which is 20s therefore it is stable in terms of roll control force. The Dutch roll mode has a large influence on the lateral stability of the aircraft as it is a short period mode in the lateral direction. If the yaw damping is low, it is seen as a difficulty in handling rather than a serious problem [14]. The damping ratio of this mode is 0.147 and the minimum value acceptable by Cook is for aircraft in cruise is 0.08. The natural frequency is 3.9 rad/s and the minimum value is 0.5rad/s therefore the handling quality is acceptable.

To further discuss the stability and dynamics of the aircraft, it was compared to an already known aircraft with similar design characteristics. The aircraft chosen for comparison was the Airbus A320 because it has a main wingspan of 35 meters and an elevator span of 12.45 meters as well as a fin height of 5.87 meters [15].

Table 2.4.4: Comparison of longitudinal modes between A320 and aircraft

	A320		Baseline Aircraft	
	Natural frequency (Hz)	**Damping ratio**	**Natural frequency (Hz)**	**Damping ratio**
Short period	0.999	0.498	0.743471	0.347696
Phugoid	0.0937	0.171	0.00920179	0.0213786
Dutch Roll	1.39	0.165	0.643293	0.147088

Using the values of natural frequency and damping ratios of the short period and phugoid modes of the two aircrafts shown in Table 2.4.4, the response was plotted shown in Figures 2.4.1 and 2.4.2 below.

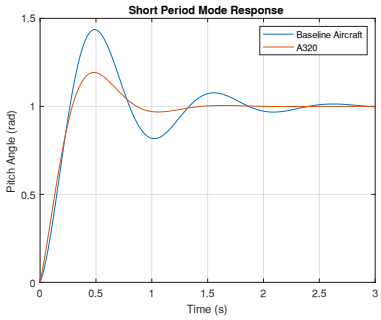

Figure 2.4.1: Response for short period mode

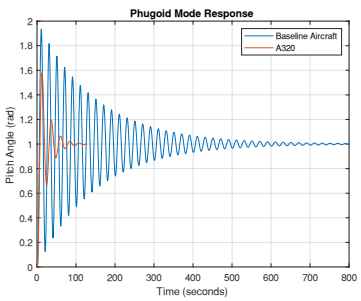

Figure 2.4.2: Response for phugoid mode

The short period and phugoid modes are both oscillatory aircraft modes. As seen in both Figures 2.4.1 and 2.4.2 the baseline aircraft has positive dynamic stability like the A320 as it settles to a certain value after a period of time. The baseline aircraft has a similar response for the short period mode as the A320 as they have similar natural

frequencies and damping ratios. They both take roughly similar times to settle, this means that the aircraft is as stable as the A320 in terms of achieving the trimmed condition after a disturbance to the pitch angle. As seen in Figure 2.4.2 above, the baseline aircraft has a settling time of almost 8 times greater than the A320 and has a much smaller damping ratio. Overall, it can be concluded that the baseline aircraft is less dynamically stable than the A320 in both the short period and phugoid longitudinal modes. For lateral modes, Figure 2.4.3 below shows the Dutch roll mode response for the A320 and the Baseline Aircraft. The A320 has a natural frequency approximately 2 times greater than the Baseline Aircraft however a similar damping ratio which is only 2% higher than the Baseline Aircraft. For both the roll and yaw angle, the A320 achieves the trimmed condition almost 5 times faster than the Baseline Aircraft as the A320 takes approximately 5-6 seconds while the Baseline Aircraft takes about 50 seconds. Both aircrafts take about 4 to 5 cycles to retrieve the stability condition.

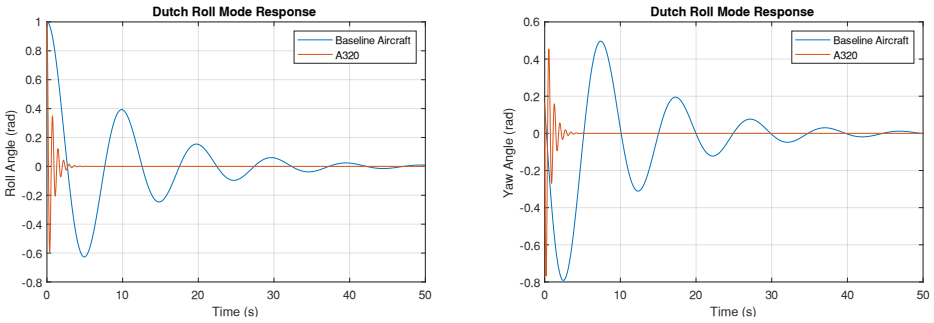

Figure 2.4.3: Dutch Roll response for roll angle and yaw angle (left to right)

5. Induced drag is calculated using the following formula:

$$D_i = \frac{1}{2}\rho V^2 S C_{D_i} \tag{6}$$

To reduce induced drag in cruise, there are several approaches in the design phase of an aircraft that could be taken. The Aspect Ratio (AR) of the wing could be increased to reduce the amount of induced drag experienced by the aircraft in cruise. This is because by increasing the AR of the wing, the wingspan typically increases which means that there is a greater distance for the air to travel to the wing tips where it sheds the vortices. These wing vortices tend to travel outwards to the wingtip and join so once the wingtip is reached there is a large wing tip vortex formed and it will shed. These vortices will increase the induced drag as explained in Q3. By increasing the wingspan there is further distance for the wing vortices to travel before shedding at the wing tip which causes the strength and size of the vortex to reduce hence the induced drag is reduced.

Another change that could be made is to alter the Taper Ratio (TR) of the wing. By increasing the taper of the wing, it means to increase the ratio of the chord at the wing root to the chord at the wing tip. If the wing has more taper, there will be less distribution of lift at the wing tip leading to smaller wing tip vortices causing less induced drag. A problem that could rise from over tapering the wing is that wing tip stall is likely to occur in highly tapered wings due to the lift distribution being at a maximum near the tip.

Additionally, the twist of the wing could be altered to reduce induced drag. By giving the wing twist, the angle of attack across the span of the wing varies. A wing is said to have ‘washout’ when the angle of incidence as the wing tip is lower than that at the wing root. This is useful because a lower angle of incidence will correspond to a lower amount of lift produced hence the drag acting against that lift is reduced. The main purpose of washout in a wing is to control the stall characteristics. By having washout, it causes the root to stall before the tip which allows the aircraft to maintain in flight without experiencing bad stall effects.

Finally, winglets could be added to reduce induced drag as they produce a forward thrust inside the circulation field of the vortices which reduce their strength [16]. With weaker vortices, induced drag is reduced and the overall efficiency of the aircraft is increased.

The parameters chosen as the design change to reduce induced drag in cruise is to change the Aspect Ratio of the aircraft. By increasing the AR, it provides more area on the wing to help reduce the wingtip vortices to reduce the induced drag. It is also the most efficient way to reduce induced drag in cruise as seen in Figure 2.5.3 the change in AR reduces C_{D_i} the most. Twist to the main wing is not added because the main wing is at an angle of incidence of 0° so inducing twist on the tip did not have a significant reduction in induced drag. Winglets were added because they showed a significant amount of induced drag reduction when added.

To change the Aspect Ratio of the aircraft, the wingspan was changed while keeping the chord of the tip the same to keep the taper ratio the same as the original aircraft so that the change in induced drag is influenced by one variable. Aspect ratio is calculated using Equation 7 where the mean geometric chord = 3.6m.

$$Aspect\ Ratio = \frac{Wingspan}{mean\ geometric\ chord} \tag{7}$$

3 iterations of aspect ratio were performed where the wingspan was increased by 7 meters from the original to the 1st iteration and 10 meters for the 2nd and 3rd iteration. As the wingspan increases, the wing area also increases which means that the MTOW will also increase proportionally. The equation from the performance section of the brief was used to calculate the new wing weight as seen in Equation 8 where S is the wing area, AR is the aspect ratio and λ is the quarter chord sweep angle. It is said that the new wing weight is proportional to the value calculated using this equation. Assuming that the wing weight is directly proportional to the MTOW seen in Equation 10, it is used to increase the MTOW to obtain the new C_l for cruise at its trimmed condition and its respective C_{D_i}. The new AR aircraft was trimmed for it to produce lift force approximately equal to the MTOW.

$$x = S^{0.65} AR^{0.5} (\cos(\lambda))^{-1} \tag{8}$$

$$x_{originalAR} = 75.375$$

$$MTOW \propto x \tag{9}$$

$$MTOW = kx \tag{10}$$

$$k = \frac{MTOW}{x_{originalAR}} = \frac{72000}{75.375} = 955.22 \tag{11}$$

This value of k calculated in equation 11 using the original MTOW and $x_{originalAR}$ is used as the constant for the following iterations whereby a new x is generated for each iteration of AR to obtain the new $MTOW$ for the trimmed cruise condition using equation 10. The values used to calculate this and the respective induced drag and lift coefficients from XFLR5 analysis are reported in Table 2.5.1, the induced drag was calculated using equation 6.

Table 2.5.1: Varied wingspan and respective aspect ratios with the C_{D_i}. The chosen design is highlighted in blue.

Iteration	AR	Wingspan (m)	wing area (m^2)	λ (°)	MTOW (N)	$C_{l_{trim}}$	C_{D_i}	Induced Drag (N), D_i
0	9.25	33.33	119.99	25	706320	0.395	0.0054	9666.2
1	11.11	40.0	144	21.23	847396.79	0.39779	0.00455	9774.5
2	13.89	50	180	17.27	1,069,265.58	0.39497	0.00359	9640.1
3	16.67	60	216	14.52	1,300,867.453	0.40889	0.00321	10343.7

A graph of induced drag coefficients and aspect ratio was plotted in figure 2.5.1 and the corresponding induced drag values were also plotted in figure 2.5.2. It can be seen that even though the design with the greatest aspect ratio has the lowest C_{D_i}, its corresponding induced drag value is much larger than even the original aircraft. This is due to the wing area being extremely large, the coefficient of drag doesn't have as much of an influence on the drag value as anticipated. Therefore the 2nd design iteration was chosen with the aspect ratio of 13.89 because the Induced drag coefficient decreases by 33.5% and induced drag reduces by 0.27%.

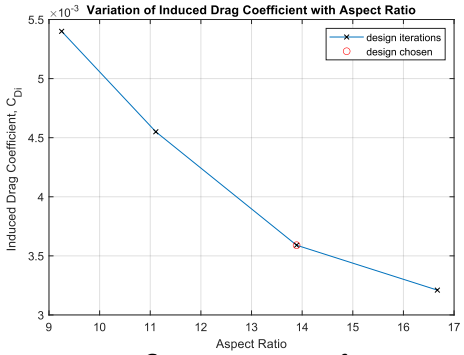

Figure 2.5.1: C_{D_i} per iteration of Aspect Ratio

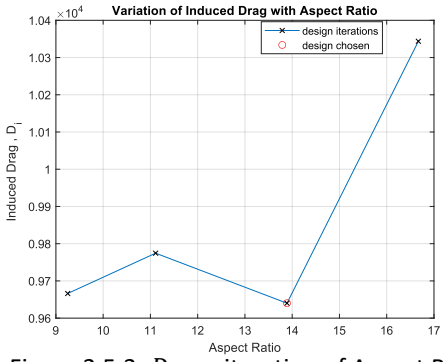

Figure 2.5.2: D_i per iteration of Aspect Ratio

After obtaining the optimal aspect ratio, the winglets on the aircraft were added to this design. The dimensions of them are described in the dimensioned diagram in figure 2.5.5. the induced drag coefficients were tested for different angles of the winglets offset from the vertical: 0°, 30° and 60°. The addition of winglets does cause the aspect ratio and wing area to increase however it is assumed that this does not increase the MTOW by a significant amount. Therefore, the values for each iteration of winglet angle are reported in Table 2.5.2.

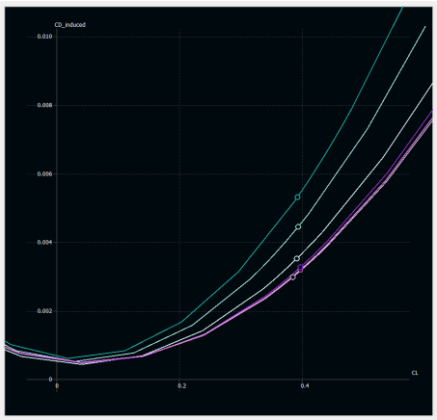

Figure 2.5.3: C_{D_i} against C_l graph from XFLR5 showing the effect of changing the aspect ratio (green shades) and adding winglets (purple shades)

Table 2.5.2: Summary of values used to obtain the induced drag.

winglet angle °	S	$C_{l_{trim}}$	alpha	C_{D_i}	D_i	$C_{D_{viscous}}$
0	187.202	0.40362	2.64	0.00338	9439.384825	0.00690
30		0.40345	2.66	0.00331	9243.894607	0.00677
45		0.39039	2.52	0.00307	8573.64243	0.00670
60		0.39418	2.56	0.00311	8685.35	0.00667

After performing 4 iterations of winglet angles it was found that the angle of 45° produced a minimum induced drag coefficient and induced drag value. As the winglet angle increased past 45° it is noticed that the C_{D_i} starts to increase again. Therefore, the angle of 45° was chosen as the optimal design iteration because the induced drag coefficient and induced drag reduces by 9.2% overall. Graphs of the progression of induced drag coefficient and induced drag against winglet angle are plotted in figure 2.5.4 and 2.5.5 respectively.

After running a stability analysis for each of the planes with varying winglet angles, it is seen from table 2.5.3 that there are slight changes to the dynamic stability modes. Comparing the modes of the final design to that of question 4, it can be seen that the short period ω_n reduces by 13.4%, phugoid ω_n increases by 19.5% and Dutch roll reduces by 15.2%. The roll subsidence eigenvalue becomes more negative and spiral mode becomes slightly more positive. This means that the overall dynamics stability remains fairly the same, but the responses of the modes will differ for the oscillatory modes. For the non-oscillatory modes, the stability improves as they are placed better in the top left corner of the s-plane based on their eigenvalues.

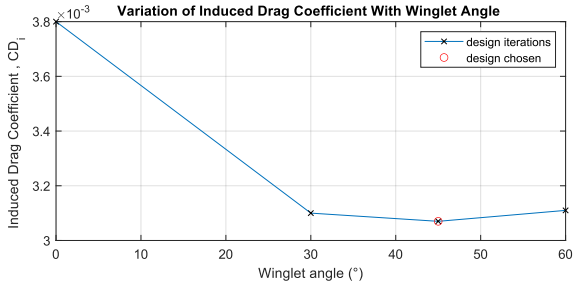

Figure 2.5.4: C_{D_i} vs winglet angle

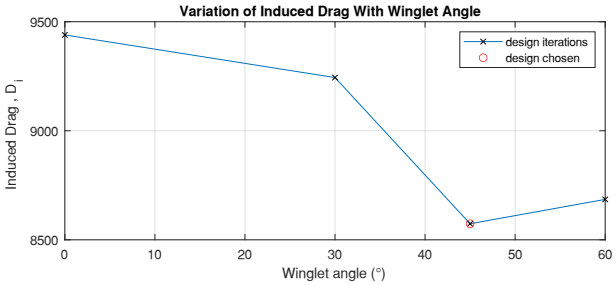

Figure 2.5.4: D_i vs winglet angle

Table 2.5.3: Summarising the dynamic aircraft modes for each AR. $\omega_n = natural\ frequency, \zeta = damping\ ratio$

Winglet angle (°)	Short period		Phugoid		Dutch roll		Roll subsidence	Spiral
	ω_n (Hz)	ζ	ω_n (Hz)	ζ	ω_n (Hz)	ζ	Eigenvalue	Eigenvalue
0	0.614537	0.389	0.011045	0.016	0.483877	0.132	-6.646 + 0.00i	-0.0004 + 0.00i
30	0.626673	0.381	0.011895	0.016	0.541975	0.155	-7.106 + 0.00i	-0.0008 + 0.00i
45	0.643537	0.378	0.011066	0.016	0.545788	0.157	-7.474 + 0.00i	-0.0006 + 0.00i

Table 2.5.4: Summarising the points of stability for each AR. MAC =3.852

Winglet angle	Neutral point (m)	CoG X (m)	Static margin (m)	% of MAC
0	18.188	16.98	1.208	31.36
30	18.243		1.263	32.78
45	18.269		1.289	33.46

The static stability of the aircraft with the variation of winglet angle is shown in Table 2.5.4. As the winglet angle increases, the neutral point increases resulting in the static margin increases. Comparing the static margin as a percentage of MAC with that of the original aircraft from question 4, the value reduces from 48.7% to 33.46% which is a 31.3% reduction showing that the elevator authority is improved with this final design.

The Oswald Efficiency Factor e was recalculated for the new optimised design which is 0.977 while the original design is 0.95. Since the new value is closer to $e = 1$ which is for an ellipse, the new value is better as an elliptic lift distribution produces less drag.

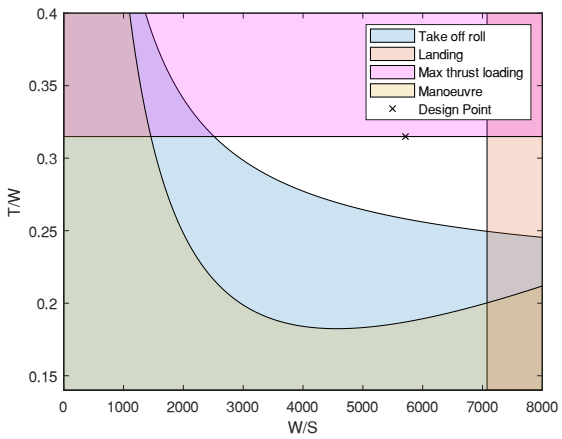

Figure 2.5.4: updated constraint diagram

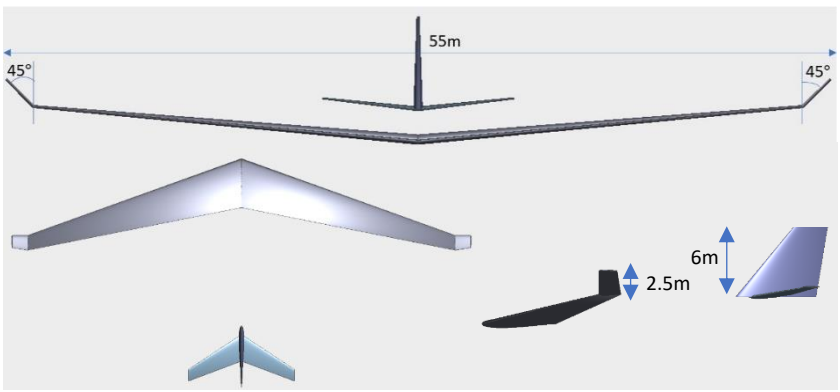

Figure 2.5.5: dimensioned diagram showing changes made.